

Institutionen för systemteknik

Department of Electrical Engineering

Examensarbete

Train localization and speed estimation using on-board inertial and magnetic sensors

Examensarbete utfört i reglerteknik
vid Tekniska högskolan vid Linköpings universitet
av

Mikael Hammar, Erik Hedberg

LiTH-ISY-EX--15/4893--SE

München 2015



Linköpings universitet
TEKNISKA HÖGSKOLAN

Train localization and speed estimation using on-board inertial and magnetic sensors

Examensarbete utfört i reglerteknik
vid Tekniska högskolan vid Linköpings universitet
av

Mikael Hammar, Erik Hedberg

LiTH-ISY-EX--15/4893--SE

Handledare: **Oliver Heirich**
 KN, DLR
Benjamin Siebler
 KN, DLR
Michael Roth
 ISY, Linköpings universitet

Examinator: **Fredrik Gustafsson**

München, 11 september 2015



Avdelning, Institution
Division, Department

Communication and navigation
Department of Electrical Engineering
SE-581 83 Linköping

Datum
Date

2015-009-11

Språk

Language

Svenska/Swedish

Engelska/English

Rapporttyp

Report category

Licentiatavhandling

Examensarbete

C-uppsats

D-uppsats

Övrig rapport

ISBN

ISRN

LiTH-ISY-EX--15/4893--SE

Serietitel och serienummer

Title of series, numbering

ISSN

URL för elektronisk version

<http://urn.kb.se/resolve?urn=urn:nbn:se:liu:diva-XXXXXX>

Titel

Title

Train localization and speed estimation using on-board inertial and magnetic sensors

Författare Mikael Hammar, Erik Hedberg
Author

Sammanfattning

Abstract

Positioning systems for trains are traditionally based on track-side infrastructure, implying costs for both installation and maintenance. A reliable on-board system would therefore be attractive. Sufficient reliability for on-board systems is likely going to require a multi-sensor solution. This thesis investigates how measurements from bogie-mounted inertial and magnetic sensors can contribute to such a system. The first part introduces and compares two different methods for estimating the speed. The first one estimates the fundamental frequency of the variations in the magnetic field, and the second one analyses the mechanical vibrations using the accelerometer and gyro, where one mode is due to the wheel irregularities. The second part introduces and evaluates a method for train localization using magnetic signatures. The method is evaluated both as a solution for localization along a given track and at switchways. Overall, the results in both parts show that bogie-mounted inertial and magnetic sensors provide accurate estimates of both speed (within 0.5 m/s typically) and location (3-5 m accuracy typically).

Nyckelord

Keywords

signal processing, railway tracks, trains, localization, speed estimation

Abstract

Positioning systems for trains are traditionally based on track-side infrastructure, implying costs for both installation and maintenance. A reliable on-board system would therefore be attractive. Sufficient reliability for on-board systems is likely going to require a multi-sensor solution. This thesis investigates how measurements from bogie-mounted inertial and magnetic sensors can contribute to such a system. The first part introduces and compares two different methods for estimating the speed. The first one estimates the fundamental frequency of the variations in the magnetic field, and the second one analyses the mechanical vibrations using the accelerometer and gyro, where one mode is due to the wheel irregularities. The second part introduces and evaluates a method for train localization using magnetic signatures. The method is evaluated both as a solution for localization along a given track and at switchways. Overall, the results in both parts show that bogie-mounted inertial and magnetic sensors provide accurate estimates of both speed (within 0.5 m/s typically) and location (3-5 m accuracy typically).

Acknowledgments

First and foremost we would like to thank Oliver Heirich and Benjamin Siebler, our supervisors at DLR, for their help and guidance. They have been positive, encouraging and interested in our work throughout our stay at DLR.

We are also grateful to rest of the RCAS guys at DLR for letting us experience the hard work of collecting data in scenic settings, as well as to the students at DLR for making our time in München so memorable.

Our thanks also go out to our university supervisor Michael Roth for his support, for his candid guidance and for taking on the difficult task of long-distance supervising.

And lastly, we would like to thank our professor Fredrik Gustafsson for making this thesis possible.

*Linköping, September 2015
Mikael Hammar and Erik Hedberg*

Contents

1	Introduction	1
1.1	Background	1
1.2	Structure	2
1.3	Related work	2
2	Datasets	5
2.1	Sensors	5
2.2	Train runs	6
I Estimation of Speed		
3	Preliminaries	9
3.1	Magnetometer	9
3.2	IMU	11
3.3	Campbell diagram	12
4	Methods	15
4.1	Wheel turn extraction	15
4.1.1	Speed estimation method	16
4.2	Signature matching	17
4.2.1	Creating the signal bank	17
4.2.2	Speed estimation	18
4.3	Kalman filtering of the obtained speed measurements	19
4.3.1	Dynamics	20
4.3.2	Measurement model	20
4.3.3	Outlier rejection	21
5	Results	23
6	Discussion	29
6.1	Wheel turn extraction	29
6.2	Signature matching	30

6.3 Filter	31
II Estimation of Location	
7 Preliminaries	35
7.1 Overview	35
7.1.1 Targeted localization problems	36
7.2 Theory	36
7.2.1 Signature creation	36
7.2.2 Similarity measures	37
7.3 Geomagnetic field	37
8 Methods	39
8.1 Signature creation	39
8.1.1 Magnetic magnitude	40
8.1.2 Temporal low-pass filtering	40
8.1.3 Transformation to spatial domain	40
8.1.4 Spatial resampling	41
8.1.5 Highpass-filtering	42
8.2 Signature matching	43
8.2.1 Similarity measures	44
8.3 Along-localization	45
8.3.1 Localization signature length	45
8.3.2 Search radius	45
8.4 Across-localization	45
8.5 Reference position	46
8.5.1 Map-matching	46
9 Results	47
9.1 Signature quality	47
9.1.1 Disturbances	47
9.1.2 Periodicity of features	47
9.2 Along localization	50
9.2.1 Effect of localization signature length and search radius . .	50
9.2.2 Comparison between similarity measures	50
9.2.3 Impact of map-matching	52
9.3 Across localization	53
10 Discussion	55
10.1 Along localization performance	55
10.2 Across localization performance	55
10.3 Disturbances	56

III Concluding remarks

11 Concluding remarks	59
11.1 Summary	59
11.2 Future work	60
11.2.1 Wheel maintenance	60
11.2.2 Estimated speed as input in the localization	60
11.2.3 Dynamic similarity measures	60
11.2.4 Pattern recognition	60
11.2.5 Incorporate inertial signals in the localization	60
A Sensor setup and technical data	63
Bibliography	67

1

Introduction

This thesis investigates how measurements of acceleration and magnetic field from a bogie-mounted sensor can contribute to estimation of train speed and location.

1.1 Background

Today most systems for train localization rely on some kind of infrastructure component, quite literally providing a highly reliable *ground truth*. This is important for the safety-conscious railway industry. But the infrastructure requirements also make such systems expensive to install and to maintain.

A purely on-board localization system would therefore be very attractive to railway operators, if it could match the reliability of an infrastructure-based system. Achieving such performance seems like a very real possibility considering the state of localization in other domains and the low degree of freedom in train movement.

In addition to infrastructure cost savings and possible gains in safety, reliable and accurate on-board localization would also open up possibilities for denser and possibly more automated railway traffic.

The desired degree of reliability most likely requires a multi-sensor solution where estimates from different sources are merged. This type of system is currently researched by the Department for Communication and Navigation at the German Aerospace Center (DLR) in Oberpfaffenhofen, and this thesis was carried out at DLR to investigate how a bogie-mounted inertial measurement unit (IMU) and magnetometer could contribute to estimation of speed and location.

A bogie is the substructure between the train body and a pair of wheel axles, allowing the wheel axles to move more freely.

1.2 Structure

This thesis deals with two topics – Estimation of speed and localization of a train using on-board sensors. Both parts follow a similar structure, namely: preliminaries, methods, results and discussion.

The estimation of speed topic deals with estimating the absolute speed based on information captured by an on-board magnetometer, gyroscope and accelerometer. The speed estimates are calculated directly by looking at snapshots of the data and thereafter fused and smoothed.

The estimation of location topic deals with estimating the one dimensional train track position based on the information captured by the magnetometer.

Before the main parts, the reader is introduced to the data used in the thesis. For the investigation real-world data is used, previously collected by DLR from a commuter train in regular traffic over the course of a month.

To conclude, the findings are summarized followed by an overview of promising areas for future work.

1.3 Related work

The work in this thesis can be seen as a continuation of work at DLR showing that it should be possible to use inertial measurements, see Heirich et al. [2013b], and magnetic measurements, see Heirich and Siebler [2015], for speed and location estimation in the ways investigated in this thesis.

Accelerometer signatures from train bogies has been used in a dual-bogie setup to estimate speed, as described in Mei and Li [2008].

Speed estimation and localization using active magnetic sensors, so called eddy current sensors, has been implemented by Hensel et al. [2011]. A method using passive magnetic measurements for localization of pedestrians in hallways, which has similarities to the railway case, is described in Subbu et al. [2011].

A different but very related and quite active area is monitoring of track condition. As tracks suffer from wear and track geometry deformation they need monitoring in order to know when maintenance is needed. When this monitoring estimates the profile and geometry of the rails it in fact performs mapping and localization, and it is thus interesting to look at these methods from a localization perspective.

A good introduction and comparison of some methods can be found in Grassie [1996]. Track monitoring is usually done by special purpose trains, but using regular in-service trains instead is of course desirable. Such systems are already in place on some Japanese Shinkansen, described in Tsunashima et al. [2012].

Promising results using a bogie-mounted solution are presented in Weston et al. [2007].

2

Datasets

The data used in this thesis was collected at a measurement campaign organized by DLR and Bayerische Regiobahn (BRB) and was used to determine speed and localization features in Heirich and Siebler [2015].

2.1 Sensors

The data comes from an Inertial Measurement Unit (IMU) containing multiple sensors and a GNSS receiver both mounted on a BRB commuter train. For reference, a dashcam was also mounted in one of the two driver cabins.

The IMU sensors consist of a three axes accelerometer, gyro and magnetometer. The sensors were sampled with 200 Hz and output sensor readings in all axes (9 outputs in total) and the corresponding timestamp for the sampled value.

The IMU was placed so that the x -axis of the sensors pointed along the the train (when the train was moving forwards) and z -axis downwards (see Figure A.1 for placement and placement data, and A.2 for technical data of the sensor).

A GNSS receiver was mounted on top of the train with a update frequency of 1 Hz. The GNSS-receiver output contained:

- Position estimate.
- Position standard deviation.
- Speed estimate.
- Speed estimate standard deviation.
- Time stamp of output.

The sensor placement and further details are described in Appendix A.1.

2.2 Train runs

The data was collected with a commuter train belonging to the Bayerische Regiobahn (BRB). All the data was collected using the same train over the course of a month and the train was in normal working traffic state and transporting passengers. The specifics of the train are further described in Appendix A.1.

The train travelled through 14 stations around Augsburg in south-west Germany. The total length of the runs is around 200 km.

After the data was collected, it was split into different train runs. Each run consists of a journey from a starting station to an end station, comprising possible station stops in between. In total there are around 140 different runs in the dataset.

Part I

Estimation of Speed

3

Preliminaries

In this chapter the motivations and explanations for what information could be used to estimate the absolute speed of the moving train can be found.

The sensors used to estimate the speed are the gyro, the accelerometer and the magnetometer. The gyro and accelerometer are affected by similar factors, whereas the magnetometer by other factors. Hence, the sensor readings are treated separately.

3.1 Magnetometer

There is a lot of information in the magnetic field around a moving train. To list the most prominent sources that induce changes in the magnetic field along the train we have

- the geomagnetic field,
- powerlines,
- DC-currents,
- environmental objects and
- noise.

The components can be visualized by looking at a frequency power transform in short time intervals – the spectrogram (see [Gustafsson et al., 2011, p. 9]) – of a longer signal.

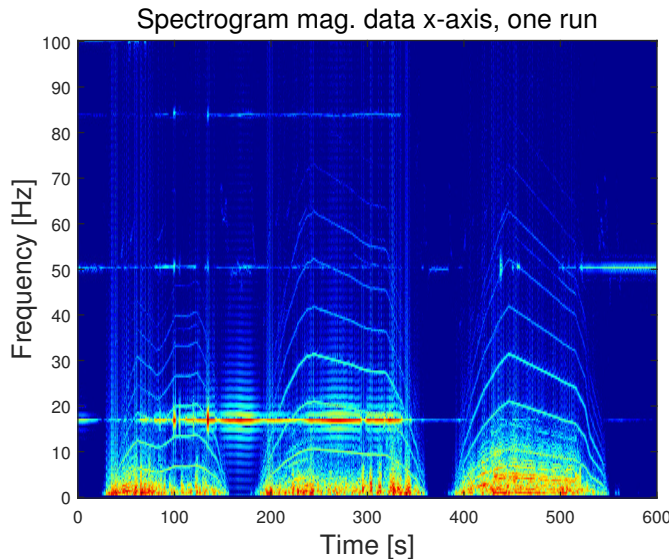


Figure 3.1: Spectrogram of magnetometer data in x-axis (along the tracks). There are visible power peaks in some frequencies.

The disturbances from the powerlines (16.7 Hz with harmonics) are prominent and the noise up to around 15 Hz as well.

The train itself also affects the magnetic field. In Heirich and Siebler [2015] it is shown that there are periodicities in the recorded magnetic signal, which could stem from the turning rate of the wheels. This means that there are features in the magnetic field that could be used to estimate the speed of the train. The time varying trends in Figure 3.1 also suggests this.

By looking at the amplitude spectrum for a specific time point and include all known factors, we get the snapshot Figure 3.2 found below.

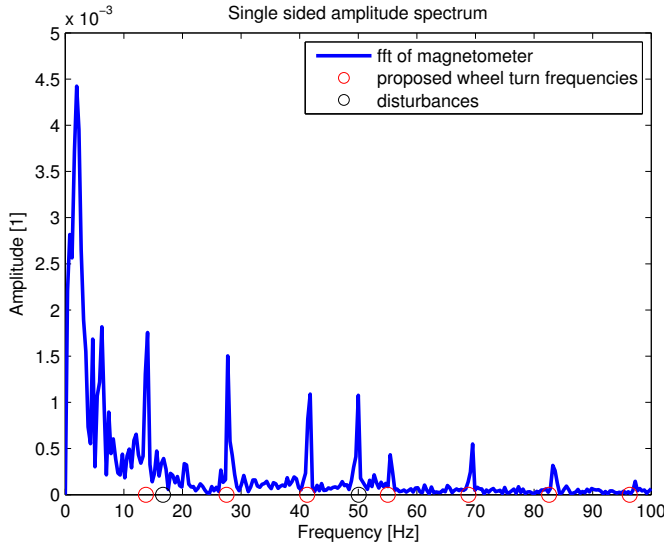


Figure 3.2: Fourier transform of a short sample (400 data points). Red circles are the expected frequencies coming from the wheel turn rate according to the GNSS-speed and the black circles correspond to the known disturbances (powerline AC with harmonics).

In Figure 3.2, the low frequency noise is visible and is prominent up to around 10 Hz. The amplitudes from the powerlines are not so prominent in this snapshot, but most importantly – the frequencies corresponding to the wheel turn rate calculated from the GNSS-speed match well.

To sum up, we have low frequency components, stationary frequency components and speed dependent components.

3.2 IMU

As for the gyro and accelerometer, they are mostly affected by

- train dynamics – how the train responds to acceleration input,
- track features – irregularities on the tracks, curves and slopes,
- vibrational sources – revolving wheels, engine and self resonance of the wagon,
- gravity and random noise.

As for the magnetic field, the IMU is proposed to be affected by periodical vibrations. As shown in Heirich et al. [2013b] and Heirich and Siebler [2015] the vibrations coming from the turning wheels could be detectable in the measured

data. It is expected that the turn rate of the wheels are detectable, but also vibrations stemming from the train wagon, springs and other on-board train sources.

By plotting a spectrogram for the same run but for the accelerometer data in the z-axis, we get Figure 3.3.

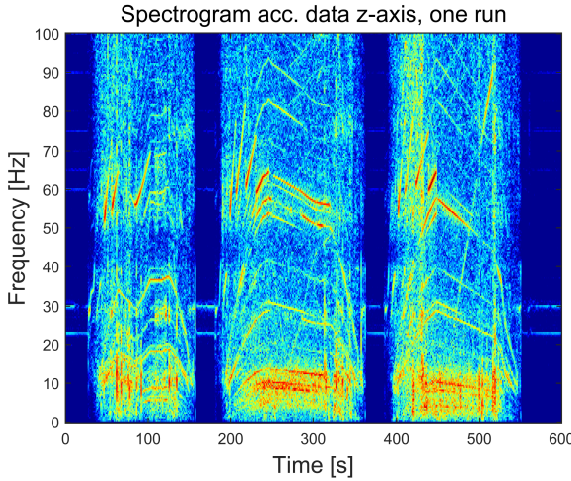


Figure 3.3: Spectrogram over accelerometer data in vertical axis (z-axis). There are time varying power peaks in some frequencies.

As seen in 3.3, there is power in many frequency bands, but some are more prominent than others. To find which frequencies are speed dependent, a Campbell diagram can be drawn.

3.3 Campbell diagram

A Campbell diagram is similar to a spectrogram, but plots power frequency spectrum against speed rather than time.

Linear speed-frequency dependencies are displayed as straight lines in the diagram and if the signals are prominent, they can be used to map a frequency signal to the corresponding speed.

By sorting 3.3 according to the GNSS-speed in Figure 3.4, the Campbell diagram 3.5 is drawn.

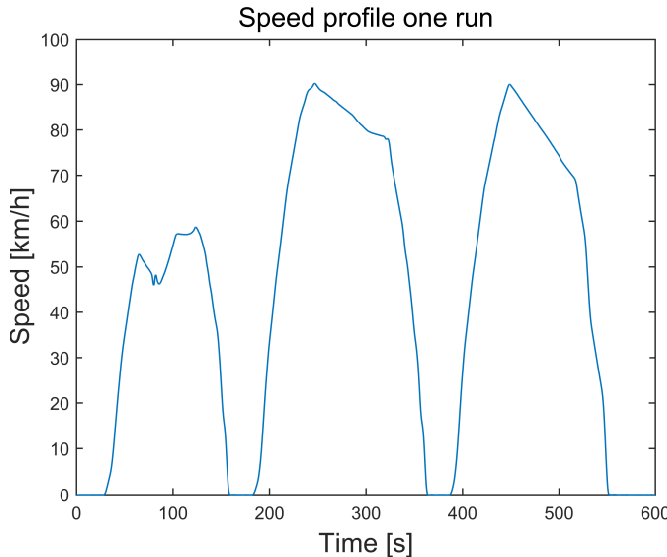


Figure 3.4: Speed profile estimated by the GNSS, which also is the speed reference used.

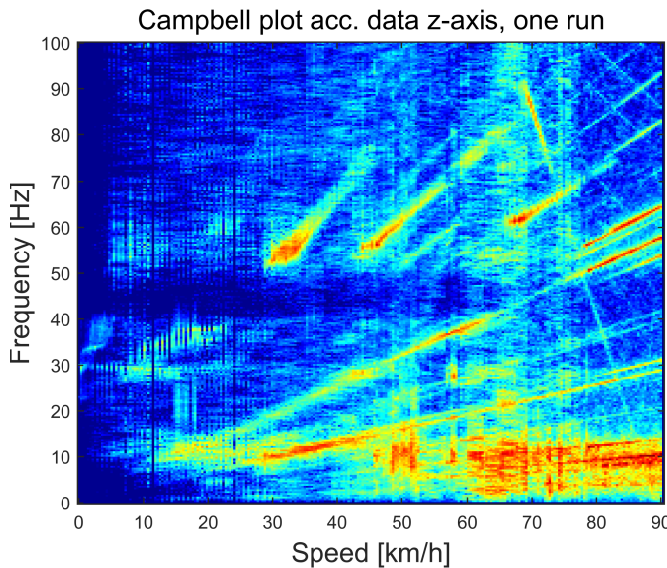


Figure 3.5: Campbell plot over the raw accelerometer data in the z-axis in one run. Linear frequency speed trends are clearly visible

By examining the Campbell plot in Figure 3.5 one can conclude there are a lot of speed-frequency dependent sources and information to be used. Since the engine is revolving with different frequencies dependent on the speed of the train, and

since the engine has gears, the relationship speed-frequency is only piecewise linear.

As there are direct speed-frequency dependencies in both the magnetometer and IMU-data, methods to create snapshot speed estimates will be investigated.

To fuse the estimates and integrate them with the dynamics of the train, a Kalman filter is implemented and used.

4

Methods

As seen in the previous chapter, sensor readings from the IMU are vastly different from the magnetometer. The most prominent source of speed information recorded by the magnetometer is the turning rate of the wheel, whereas the gyro and accelerometer are mostly affected by mechanical vibrations.

Using the features, two methods are developed – one where the turn rate of the wheel is extracted from the magnetometer data (wheel turn extraction) and one where all the features from the IMU are used to match the current output signal from the IMU to a specific speed (signature matching).

4.1 Wheel turn extraction

The main idea to extract the turn rate of the wheel is to find the frequencies in the magnetometer that correspond to the proposed wheel turn rate frequencies. Since the wheels of the train are irregular, it is proposed that there will be periodic changes in the magnetic field when the train is travelling. With a constant velocity v m/s and a wheel diameter d m, the wheel will have a turning period time of $T_w t = \frac{d\pi}{v}$.

Since it unknown how many irregularities there are, it is proposed that the frequencies induced in the magnetic field will correspond to the fundamental wheel turn period $T_w t$, as well as harmonics of it, yielding

$$f_{\text{nwt}} = n \frac{v}{d\pi}, n = 0, 1, 2, \dots, \quad (4.1)$$

where n are the harmonics.

Apart from the frequencies stemming from the turn rate of the wheel, we have stationary frequencies coming from the powerlines (16.7 Hz with harmonics) and low frequency noise. The power of the signal in the frequency bands around the powerline frequencies varies unpredictably with time and are hence hard to filter away easily.

All in all, the data in the magnetometer consists of a speed dependent part (the turning wheels) and frequency specific disturbances (AC, DC, low frequency noise).

4.1.1 Speed estimation method

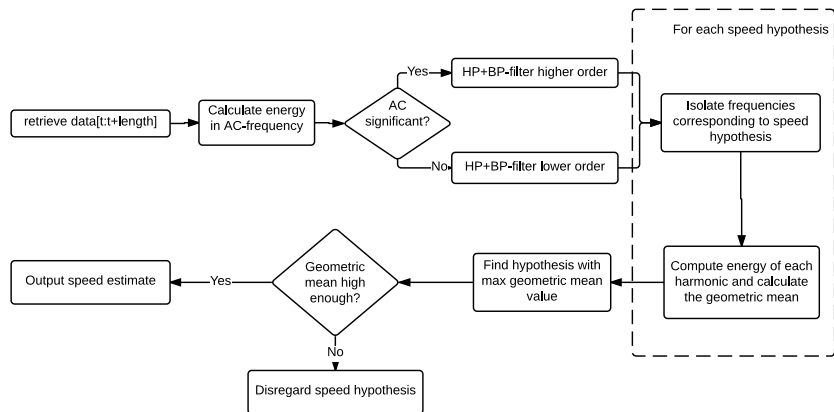


Figure 4.1: Flowchart for estimating the speed by extracting the wheel turns.

A flowchart of the method can be seen above in Figure 4.1, and the steps are explained in greater detail below.

A sample of 2s (400 pts) in the x -direction (along the direction of the train) of the magnetometer is buffered and pre-processed by a high pass filter with cut-off around 17 Hz to attenuate the noise, and a multi band stop filter with cut-off frequencies around $16.7k$ Hz, $k = 1, 2, 3, \dots$, to attenuate the known disturbances.

To decide the order of the filters, a threshold $T_{\text{threshold}}$ is set in comparison with $\frac{E_{\text{AC}}}{E_{\text{tot}}}$. If $\frac{E_{\text{AC}}}{E_{\text{tot}}} < T_{\text{threshold}}$ higher order filters are used, else corresponding filters with lower order are used.

After the noise and disturbances are suppressed, the frequencies corresponding to the wheel turn rate are isolated by letting the sample be filtered through multiple notch-filters (by filtering in the frequency domain) corresponding to each speed hypothesis v_{hyp} .

The multiple notch-filter is a band pass filter, allowing the wheel turn frequencies $f_n = (n+1) \frac{v_{hyp}}{d\pi}$, $n = N_0, N_0 + 1, N_0 + 2, \dots, N$ to pass unattenuated, corresponding to the speed hypotheses v_{hyp} gridded from a lowest speed v_{min} to a maximum of v_{max} with a desired resolution. Since the train speed never exceeds 35 m/s, this is set as v_{max} . To tune the algorithm, v_{min} , N and N_0 can be set. As the energy from the turn rate of the wheels are low for low speeds, empirical studies have shown that setting it lower than 5 m/s does not improve the estimates and can therefore be seen as a lower bound.

As a measure of how good the speed hypothesis is, the geometric mean

$$E_{v_{hyp}} = \sqrt[N]{\prod_{k=0}^{N-1} E_{f_k}}, \quad (4.2)$$

where E_{f_k} is the energy around f_k , is calculated for each filtered output. The maximum is then used to estimate the speed.

4.2 Signature matching

Since the frequency response for a certain speed is very characteristic, as seen in the Campbell plot in Figure 3.5, the idea is to match each frequency response to a certain speed.

In order to do so, a bank of pre-recorded signals is needed. The bank is created by recording a piece of the signal and store the signal with the corresponding speed as described in Section 4.2.1.

The speed can then be identified by matching the signal with the bank, which is described in Section 4.2.2. The signal in the bank that matches the best with the buffered signal can then be used to estimate the speed.

4.2.1 Creating the signal bank

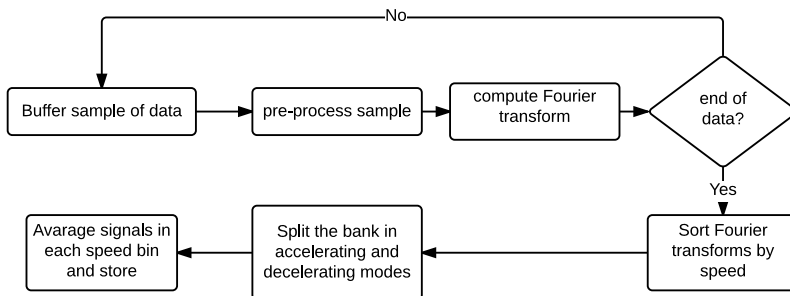


Figure 4.2: Flowchart creating the signal bank

To create the bank of speed-frequency dependencies, the accelerometer data in the z-axis and gyro data in the x-axis for each run are pre-processed, transformed into the Fourier domain and then stored. This is done, as seen in Figure 4.2, until the complete run is done.

When the run is done, the stored signals are sorted by the estimated GNSS-speed gridded from 0-35 m/s with a resolution of 0.1 m/s and whether the train is accelerating or decelerating.

The effects of the environment and other factors are suppressed by taking the mean value of signals in the same bin (signals recorded at the same speed) and stored in the bank.

4.2.2 Speed estimation

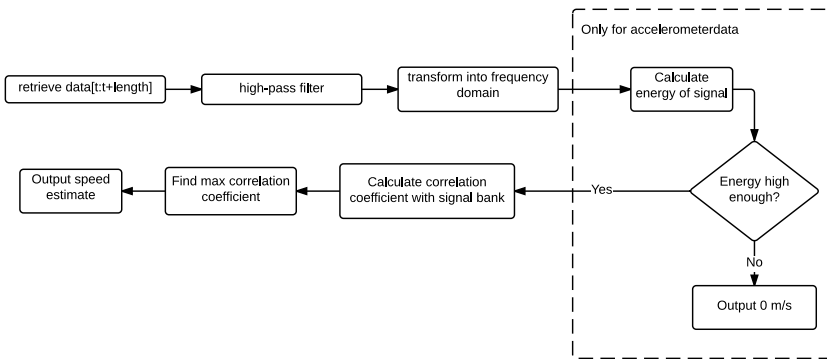


Figure 4.3: Flowchart of the signature matching method

A flowchart of the method can be seen above in Figure 4.3, and the steps are explained in greater detail below.

A sample of 2s (400 samples) of accelerometer data in the z-axis and gyro data in the x-axis data is buffered and the low frequency components are attenuated by a low pass filter with cut-off frequency around 15 Hz and order around 2. The filter must be the same as used to create the signal bank.

The energy in the signal of the accelerometer is dependent on the speed of the train – when the train is travelling fast the vibrational energy is higher. So if the energy E_{vib} of the sample is below a threshold T_{vib} , the speed estimate is 0 m/s and no further analysis is done.

On the other hand, if the energy is above the threshold T_{vib} , the current speed can be estimated by looking at the correlation coefficient $p_n(x, y_n) = \frac{\text{Cov}(x, y_n)}{\sqrt{\text{Var}(x)\text{Var}(y_n)}}$ between the sample x and each signal in the signal bank y_n to find which signal in the bank the retrieved signal matches the most.

The speed corresponding to the highest correlation is then used as an estimate of the speed.

4.3 Kalman filtering of the obtained speed measurements

After the speed is estimated by the wheel turn extraction and signature matching for all signals, the estimates are fused and smoothed with regards to the dynamics of the train as well as the noise in the measurements by a Kalman filter.

4.3.1 Dynamics

The speed of the train when looking at the speed profile follows a piecewise constant acceleration (as seen in Figure 3.4), which makes a constant acceleration model with process noise in the acceleration state suitable. The state vector z_k at time sample k can be written as

$$\mathbf{z}_k = \begin{pmatrix} x_k \\ v_k \\ a_k \end{pmatrix}, \quad (4.3)$$

where x_k is the one dimensional position of the train, v_k and a_k the speed and acceleration of the train respectively.

The dynamics can then be discretized as

$$\mathbf{z}_{k+1} = \begin{pmatrix} x_{k+1} \\ v_{k+1} \\ a_{k+1} \end{pmatrix} = \begin{pmatrix} 1 & T & \frac{T^2}{2} \\ 0 & 1 & \frac{T}{2} \\ 0 & 0 & 1 \end{pmatrix} \mathbf{z}_k + \begin{pmatrix} \frac{T^3}{6} \\ \frac{T^2}{2} \\ \frac{T}{2} \end{pmatrix} \mathbf{w}_k, \quad (4.4)$$

where w_k is the Gaussian process noise in a_k with $E(\mathbf{w}_k) = 0$ and $\text{Var}(\mathbf{w}_k) = Q$, with Q being a 1×1 matrix tuning parameter.

Since we have acceleration inputs at a rate of 200 Hz, the acceleration can be put as an input to the system. The acceleration state is then removed from the state vector, but since the accelerometer has a time-varying bias it is modelled and included in the state vector, yielding

$$\mathbf{z}_k = \begin{pmatrix} x_k \\ v_k \\ a_k^b \end{pmatrix}. \quad (4.5)$$

The dynamics can then be described as

$$\mathbf{z}_{k+1} = \begin{pmatrix} x_{k+1} \\ v_{k+1} \\ a_{k+1}^b \end{pmatrix} = \begin{pmatrix} 1 & T & \frac{T^2}{2} \\ 0 & 1 & \frac{T}{2} \\ 0 & 0 & 1 \end{pmatrix} \mathbf{z}_k + \begin{pmatrix} \frac{T^2}{2} \\ \frac{T^3}{6} \\ \frac{T^2}{2} \end{pmatrix} \mathbf{a} + \begin{pmatrix} \frac{T^3}{6} \\ \frac{T^2}{2} \\ \frac{T}{2} \end{pmatrix} \mathbf{w}_k, \quad (4.6)$$

where w_k is the Gaussian process noise in a_k^b with $E(\mathbf{w}_k) = 0$ and $\text{Var}(\mathbf{w}_k) = Q$, with Q being a 1×1 matrix tuning parameter. The variance $\text{Var}(a) = Q_u$ is also a tuning parameter.

4.3.2 Measurement model

The measurement vector y is taken as wheel turn extractions from the magnetometer in x-direction and vibrations detected by the accelerometer in z-direction and gyro in x-direction (roll).

$$\mathbf{y}_k = \begin{pmatrix} m_k^x \\ a_k^z \\ g_k^x \end{pmatrix} \quad (4.7)$$

The measurements at time step k are

$$\mathbf{y}_k = \begin{pmatrix} m_k^x \\ a_k^z \\ g_k^x \end{pmatrix} = \begin{pmatrix} v_k \\ v_k \\ v_k \end{pmatrix} + \mathbf{e}_k, \quad (4.8)$$

where \mathbf{e}_k is the measurement noise with $E(\mathbf{e}_k) = \mathbf{0}$ and $Cov(\mathbf{e}_k) = R$, with R being a 3×3 matrix tuning parameter.

Since the energy of the signal is increased with increased speeds, the measurements are more reliable when the train is moving faster. The measurements from the magnetometer are generally unreliable when the train is going slower than 10 m/s, so the covariance matrix R can be split up in three different scenarios:

- R_{still} (for speeds ≈ 0 m/s),
- R_{slow} (for speeds > 0 m/s and < 10 m/s) and
- R_{fast} (for speeds > 10 m/s).

Structuring the dynamics and measurements as

$$\begin{aligned} \mathbf{z}_{k+1} &= A_k \mathbf{z}_k + G_k \mathbf{w}_k, \\ \mathbf{y}_k &= C_k \mathbf{z}_k + \mathbf{e}_k, \end{aligned} \quad (4.9)$$

where A_k and G_k are defined as the matrices in (4.4) and C_k by (4.7) and the covariances of \mathbf{w}_k and \mathbf{e}_k are subject for tuning, the Kalman filter algorithm can be performed recursively as in [Gustafsson, 2012, p. 154].

4.3.3 Outlier rejection

The estimates contain a lot of outliers that must be detected, discarded or corrected. A way of doing that is to check whether it is plausible that the estimate error ϵ_k is normally distributed. By calculating

$$d_k^i = \sqrt{(\epsilon_k' - \mu) S_k^{-1} (\epsilon_k - \mu)}, \quad (4.10)$$

and comparing it to some threshold T_d^i we can decide whether to use the output from the method in the filter or not. If $d_k^i > T_d^i$ the measurement update of measurement i will not be executed. See [Gustafsson, 2012, p. 186-187] for further information.

5

Results

Here the results of the speed extraction methods and filtering are presented. Each plot has a smaller description of what is displayed.

The data analysed was collected for a train run around 7000 m long that had 3 station stops in total. As a speed reference, the GNSS-speed is used.

All result figures have the same structure – in the first subplot the result figures the estimates are plotted as blue and green dots, where blue dots are estimates within 0.5 m/s of the GNSS-speed reference, and the green dots estimate above. The estimates are colored for visualization. The second subplot of the figures displays the difference between the speed estimates and the GNSS-speed reference. As a measure of how good the methods are at estimating the speed, the percentage of estimates within 0.5 m/s of the GNSS-speed is displayed. For the wheel turn extraction, this value is only calculated for speeds over 10 m/s, since it only estimates speeds higher or equal to this speed. For the other methods the value is calculated in the range 0-35 m/s.

The result Figure 5.1 contains the speed estimates from the wheel turn extraction (see Section 4.1) using magnetometer data in the x-direction and Figure 5.3 and Figure 5.4 contain speed estimates from the signature matching method (see Section 4.2) using accelerometer data in the z-direction and gyro data in the x-direction (roll), respectively.

The result from fusing the estimates above with the Kalman filters described in Section 4.3 are then visualized in Figure 5.5 (using only speed measurements) and Figure 5.6 (using also train acceleration input).

For the signature matching method, the signal bank for the accelerometer data in the z-axis is visualised as a Campbell diagram (see Section 3.3 and can be found

in Figure 5.2.

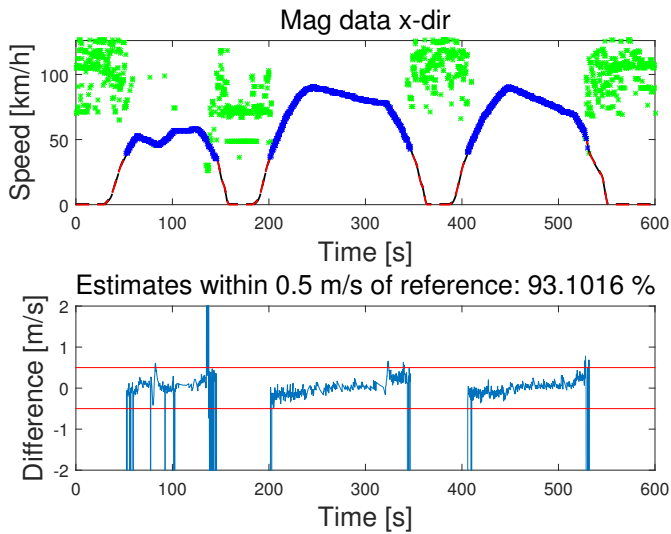


Figure 5.1: Speed estimates of the wheel turn extraction using magnetic data along the x-axis for one run. In the first subplot, blue dots represent speed estimates within 0.5 m/s of the reference, whereas green dots above and the red line GNSS-speed reference. In the second subplot, the blue line is the difference between the speed estimates and the GNSS-speed reference, with 0.5 m/s boundaries (red lines). Estimates are good for high speeds but worse for lower. For speeds lower than 10 m/s it is practically impossible to estimate the speed. Counting only estimates over 10 m/s, around 95 % of the estimates are within 0.5 m/s of the speed reference.

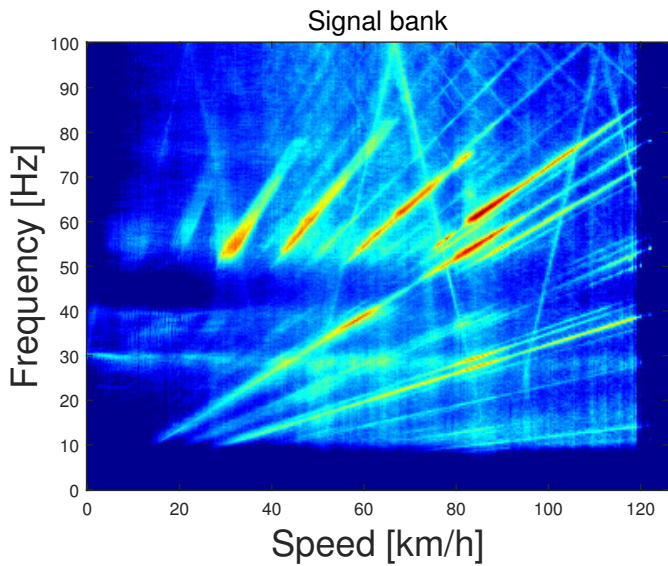


Figure 5.2: Signal bank for the accelerometer data in the z-axis created by averaging Campbell diagrams of 10 different runs. Linear speed-frequency dependencies are visible, but the lines do not match the proposed lines of the wheels and come from unknown sources.

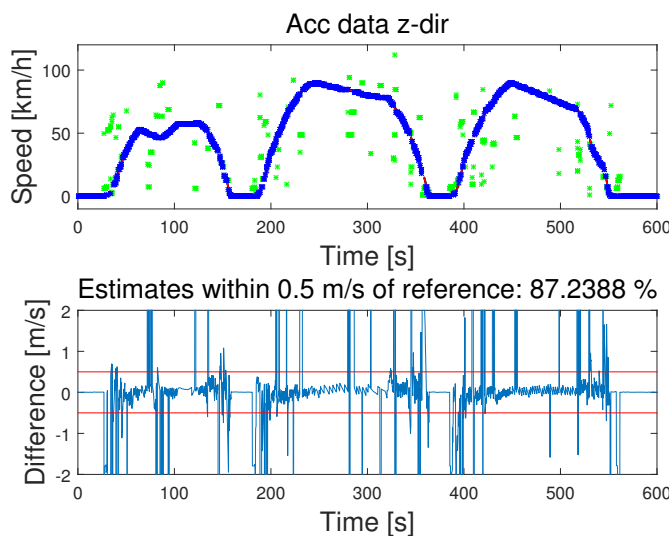


Figure 5.3: Speed estimates and errors from the signature matching method using accelerometer data along the z-axis for one run. In the first subplot, blue dots represent speed estimates within 0.5 m/s of the reference, whereas green dots above and the red line GNSS-speed reference. In the second subplot, the blue line is the difference between the speed estimates and the GNSS-speed reference, with 0.5 m/s boundaries (red lines). Speed estimation spans the whole speed range 0-35 m/s. Counting for all speeds, around 75 % of the estimates are within 0.5 m/s of the speed reference.

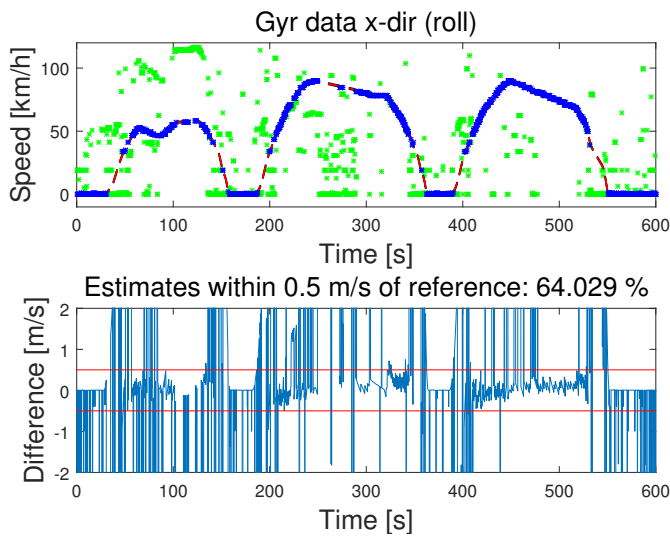


Figure 5.4: Speed estimates and errors from the signature matching method using gyro data along the x-axis (roll) for one run. In the first subplot, blue dots represent speed estimates within 0.5 m/s of the reference, whereas green dots above and the red line GNSS-speed reference. In the second subplot, the blue line is the difference between the speed estimates and the GNSS-speed reference, with 0.5 m/s boundaries (red lines). Estimates are good for high speeds but worse for lower. Counting for all speeds, around 60 % of the estimates are within 0.5 m/s of the speed reference.

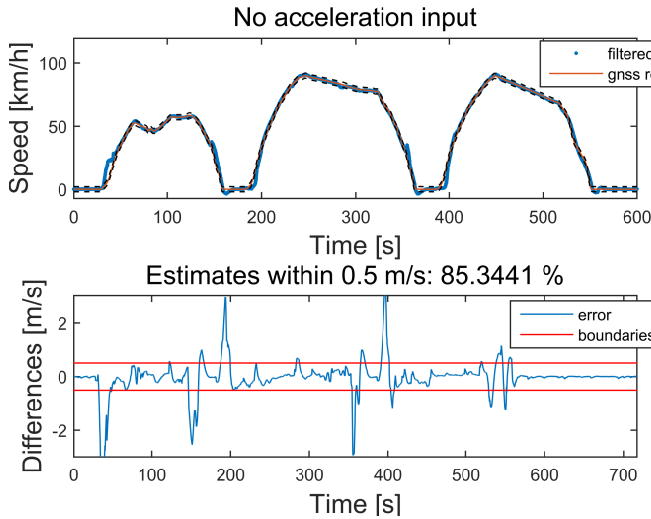


Figure 5.5: Filtered speed estimates using a Kalman filter with outlier rejection are shown. The filtered speed estimates are shown above and the difference to the GNSS-reference below. The speed estimates are good for higher speed, but worse within 0-10 m/s.

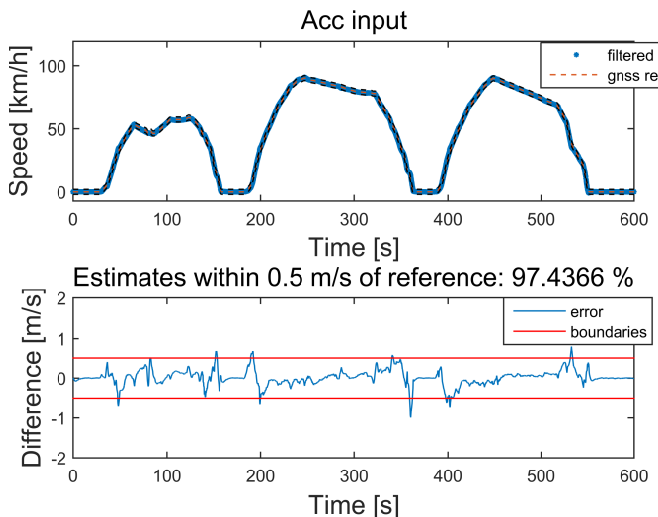


Figure 5.6: Filtered estimates using a Kalman filter with outlier rejection and acceleration input with bias in the acceleration state are shown. The filtered speed estimates are shown above and the difference to the GNSS-reference below. It can be seen that the speed estimates are improved especially for lower speeds when using the acceleration as an input.

6

Discussion

The methods of extracting speeds work well. There is enough speed dependent information in the vibrations to estimate the speed with a good enough accuracy.

6.1 Wheel turn extraction

The proposed frequencies are prominent enough in the spectrum of the magnetometer to be seen in the magnetometer data as seen in Figure 3.1.

Thus, by filtering the low frequency noise and the known disturbances, the frequencies from the wheel turn rate are prominent enough for accurate speed estimation. By results, the wheel turn extraction estimates from the wheel turn extraction method in Section 4.1 are accurate (above 90 % for speeds from 10 m/s) as can be seen in Figure 5.1.

However, the estimates are highly unreliable for speeds lower than 10 m/s. Especially when the disturbances from the powerlines strong.

To estimate the speed when the train is travelling with speeds lower than 10 m/s, more sensitive methods need to be developed. This could either be done by suppressing the AC more accurately and isolate the frequencies of the wheels better.

Another drawback is that the estimates are sometimes a harmonic of the correct speed. These measurement can be discarded as outliers by a filter but then information is wasted. Since the method gives snapshot estimates, one idea would be to output multiple hypotheses, and let some higher order filter decide which is the correct one.

6.2 Signature matching

The estimates coming from the accelerometer and gyro has a broader range (works down to 0 m/s) but is not as accurate ($\approx 70\%$).

As there are many sources of mechanical vibrations affecting the accelerometer (as seen in Figure 3.5, the correlation of the signal gets accurate enough. But since the relation speed-frequency is non-linear (only piecewise linear) the estimates can not be corrected by adjusting the estimate by an harmonic.

The estimates from the accelerometer fails when there are spikes of energy entering the measurement box, which occur when the train passes a split or some feature on the track.

The gyro is more sensitive to the disturbances as it has fewer and less prominent features, as can be seen below. Though, there is a linear dependency between speed and frequency, which causes outliers to be harmonics of the real speed and are thus subject for correction.

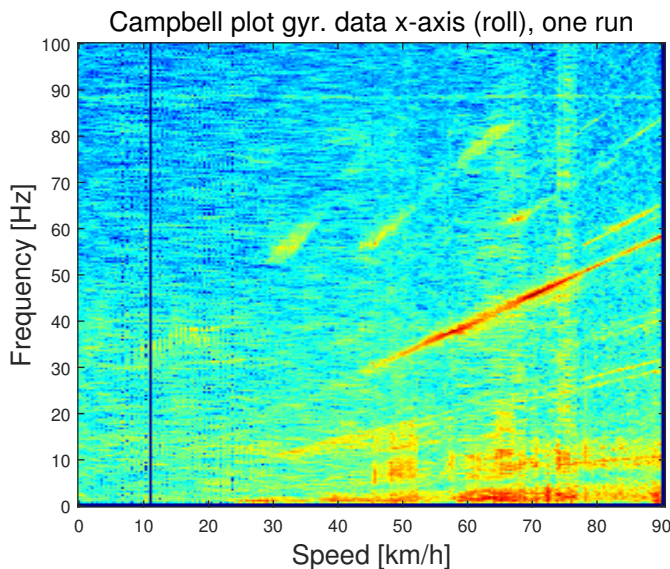


Figure 6.1: Campbell plot of one run to visualize speed-frequency features. There are some features to be used, but they are not so prominent. The speed-frequency dependency is more linear than for the accelerometer

Figure 5.3 also suggests the estimates are best when the train is either standing still or having a low acceleration. By measuring the energy in the accelerometer data one can, with high accuracy, tell whether the train is moving or not.

6.3 Filter

Filtering the estimates from the accelerometer, gyroscope and the magnetometer makes the estimates accurate enough when there are sufficient data (see Figure 5.5). The problem is that there are not that many estimates between the speeds 0 and 10 m/s, which makes the filter diverge easily and tuning the parameters hard.

To resolve the problem of too few measurements, the acceleration along the train is used as an input with simplification of no slope. Since this is not the case, the estimates coming from the accelerometer is not perfect. By introducing a bias in the accelerometer (the accelerometer is affected by a time-varying bias) the drift of the sensor is taken care of and the errors from the slope also enters the bias, making it not so apparent in the filtered measurements. The accelerometer improves the estimates, especially for lower speeds (0-10 m/s) as can be seen by comparing Figure 5.5 and Figure 5.6.

Another problem is the error distribution of the speed estimates. As the methods use non-linear operations, it is not expected that the speed estimates are normally distributed. Since the Kalman filter is the optimal filter for linear problems with normal distributions, the estimates are not optimal. Other filters could be considered to handle this problem.

There is also a problem with the speed reference. As the GNSS fails in tunnels, whereas the methods still works, the speed estimate is regarded as wrong even though it is not. It can be seen in the starting part of Figure 5.6 that the errors of the GNSS make the performance measurement worse than they are.

Part II

Estimation of Location

7

Preliminaries

7.1 Overview

The problem of estimating the location of a train differs somewhat from many other localization problems in that a train is very limited in the ways it can move, making it a problem of reduced dimensionality where the railway network can be thought of as a graph, with edges and nodes.

The needs for positioning accuracy in railway applications vary a lot, in some cases it is enough to know on which edge a train is, but in others it is vital to know the exact position to within a few meters.

Given a map of the physical rail network and a Global Navigation Satellite System receiver (GNSS) it is of course possible to solve the localization problem by taking the GNSS position and matching it to the railway network. If these positions are then filtered to incorporate the physical limitations on train movement the localization becomes quite accurate in most scenarios. However, GNSS accuracy varies significantly and suffers especially in built-up areas where many satellites are out of view, making it insufficient in safety critical applications. Another issue with GNSS is that parallel tracks can be hard to distinguish.

Beside immediate applications in safety, higher accuracy positioning would also open up long-term possibilities of more efficient and automated railway usage.

Therefore, there is an interest in investigating complementary methods to improve accuracy in railway navigation, and in this part of the thesis we propose such a method based on measuring the magnetic field. The main idea is that the magnetic field along the tracks contains enough information that measuring it allows identification of what part of tracks the measurements came from.

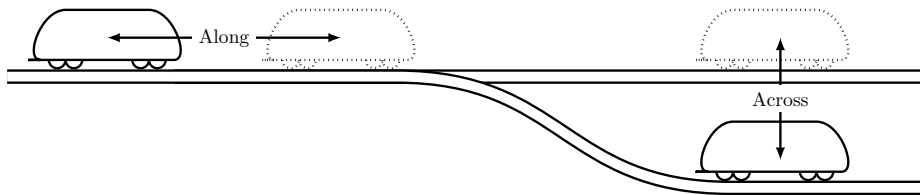


Figure 7.1: Two kinds of localization situations are considered: *Along*-localization, meaning finding position in a given area along a given track, and *Across*-localization, meaning detecting which track the train took at a given switch.

As this method is of interest primarily to augment multisensor localization systems that already implement some form of filtering based on vehicle dynamics, we have not tried to filter the location estimate. The focus is on investigating how useful this approach is as a "raw" location estimate.

7.1.1 Targeted localization problems

We focus on achieving good localization accuracy in two situations of special interest as complements to existing solutions:

- Localization along a known track segment.
- Detection of which track was chosen at a known railway switch.

The two situations are illustrated in Figure 7.1.

7.2 Theory

Localization will be performed by extracting a so called signature from the measurements and finding a similar subsequence in a previously collected reference signature, referred to as a map, in which each datapoint is associated with a known location.

7.2.1 Signature creation

Two properties are desired from signatures in this scenario:

- A signature should be as unique as possible with regard to location, i.e. two subsequences of a signature should only be similar if they are associated with the same position.
- Signatures created from different measurements over the same path should be as similar as possible, i.e. they should ideally be insensitive to time-variant factors and only represent location-dependant information.

The above makes it clear that the question of how to measure similarity is as important as how to create the signatures.

7.2.2 Similarity measures

Several standard similarity measures for data series have been described in literature, such as correlation, the L_2 - or Euclidian norm, the L_1 -norm, Dynamic Time Warping (DTW) and Longest Common Subsequence (LCSS). The latter two are so called dynamic measures; the data sequence can be distorted in order to get better fit. This makes such measures suitable for handling data recorded at different speeds or with distortions in the time- or distance-base. For a well-written overview and comparison of similarity measures in the context of time series comparison, see Ding et al. [2008]. An illustrative introduction to DTW can be found in Müller [2007].

No similarity measure is inherently better, it is only a question of which measure performs best in the application at hand. Therefore, different similarity measures must be evaluated in parallel with different signature creation methods.

7.3 Geomagnetic field

The earth's magnetic field in the Augsburg area during January 2014 is, according to the International Geomagnetic Reference Field (see NOAA [2015]), estimated to have been around 48 250 nT. The field strength globally varies in the range of 22 000 to 67 000 nT, for a more detailed description of the global geomagnetic field, see Chulliat et al. [2015]. The local earth magnetic field varies with time, which is something to keep in mind when reasoning about magnetic signatures for localization. There are several causes for these variations:

- Day/Night cycle - 20 nT, variations of up to 70 nT.
- Solar activity - Irregularly occurrence and strength, 100 nT not uncommon.
- Changes in the global earth magnetic field - slow change in direction and magnitude. In the Augsburg area currently an increase of around 29 nT per year.

As these are fluctuations that occur over large areas, they should not be a significant factor as long as the signal is detrended or highpass-filtered. The Geomagnetic Observatory Fürstenfeldbruck (IAGA-code FUR) is located at 34 km from Augsburg, and should provide a good indication of temporal variations in the magnetic field in Augsburg. Figure 7.2 shows measurements recorded at Fürstenfeldbruck during January 2014.

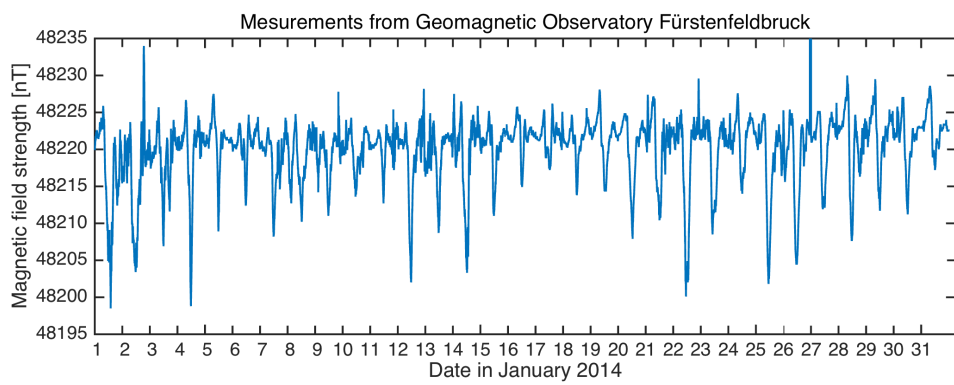


Figure 7.2: Measurements of the geomagnetic field from the Fürstenfeldbruck Geomagnetic Observatory (IAGA-code FUR). Note the clear 24h-cycles with minima during daytime.

8

Methods

This chapter describes the methods developed for localization. First methods for creating and matching magnetic signatures are described, then we show how these methods are used to perform along- and across-localization. Lastly, methods used in the evaluation are described.

8.1 Signature creation

The signature is a spatially sampled signal derived from measurements of the magnetic field, it can be thought of as a map of the magnetic environment along the tracks. An overview of the signature creation is given by Figure 8.1. The different steps in signature creation, and the considerations involved, are described in the following subsections.

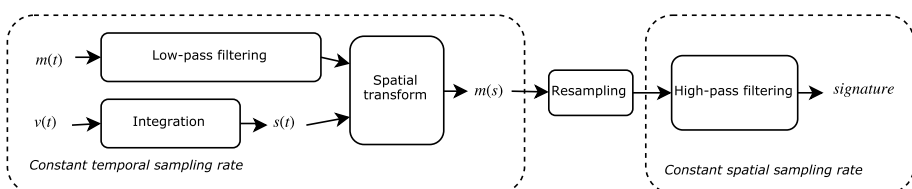


Figure 8.1: The signature is a signal of constant spatial sampling, obtained from measurements of the magnetic field and of the velocity, both sampled at constant temporal rate.

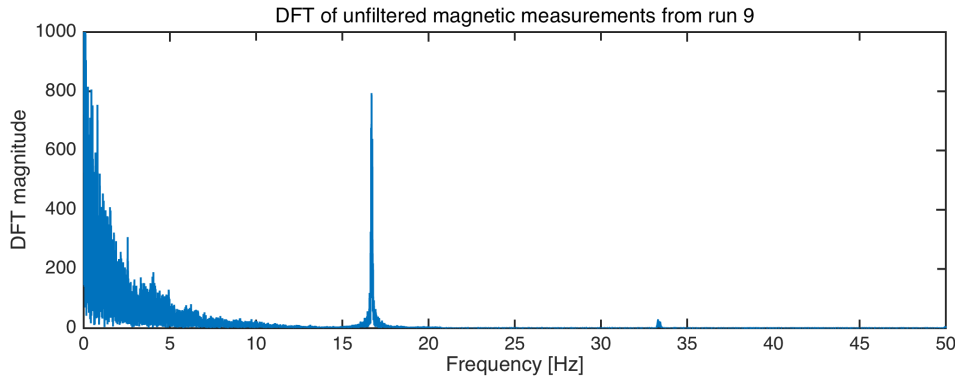


Figure 8.2: High-frequency energy, thought to arise mainly from time-dependent features instead of location-dependent features, is filtered out.

8.1.1 Magnetic magnitude

First, the magnetic measurements are used to calculate the absolute value of the magnetic field vector, called the magnetic magnitude. This makes the signal less dependent on the orientation of the sensor.

8.1.2 Temporal low-pass filtering

To remove high-frequency disturbances to the ambient magnetic field, e.g. from the electric equipment in the railway environment, the magnetic magnitude is then low-pass filtered.

The temporal filter must be chosen so that location dependent features in the signal are preserved as much as possible even when the train has a high speed. Therefore it is instructive to look at the spatial wavelength corresponding to the chosen cut-off frequency at maximum speed. As the maximum speed in the dataset does not exceed 35 m/s, the following calculation shows that a cut-off frequency of 15 Hz equals a spatial cut-off wavelength of 2.33 m at most:

$$35 \cdot \frac{\text{meters}}{\text{second}} \Bigg| 15 \cdot \frac{\text{samples}}{\text{second}} = 2.33 \cdot \frac{\text{meters}}{\text{sample}} . \quad (8.1)$$

Of course, a signature with a high spatial frequency is desirable since it will contain more location information, but this has to be weighed against how detrimental time-dependent signal components like the railway AC are.

8.1.3 Transformation to spatial domain

As the signature is to be a kind of spatial map containing information of the magnetic field along the tracks, the signal needs to be parametrized by distance instead of time. That is, each filtered sample has to be matched to a spatial posi-

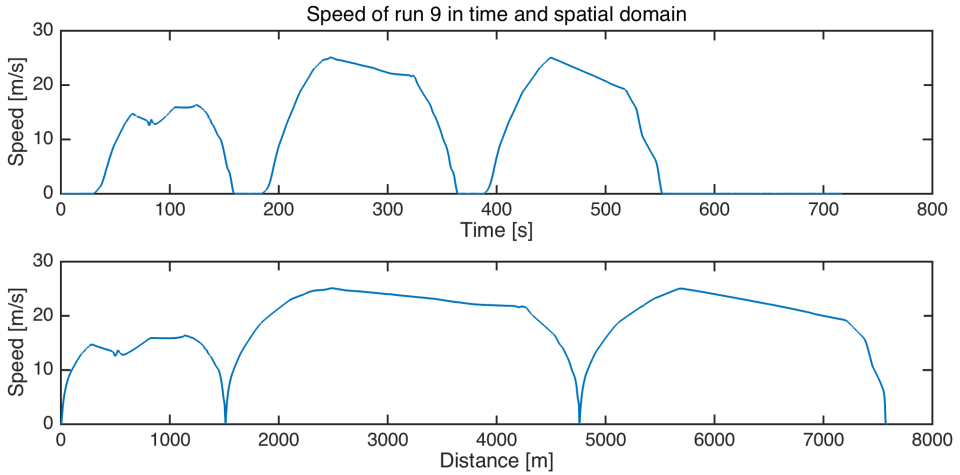


Figure 8.3: The first step in the spatial transform is using the travelled distance as base instead of time.

tion (travelled distance) \mathbf{d} .

For the first sample \mathbf{d} is set to zero and the subsequent distances are simply obtained by integrating a speed estimate \mathbf{v} (from GNSS or other sources) in the following way:

$$d_i = \begin{cases} 0 & \text{if } i = 0 \\ d_i + (t_i - t_{i-1}) \cdot v_{i-1} & \text{if } i > 0 \end{cases} \quad (8.2)$$

The result is illustrated in Figure 8.3.

Of course, if the travelled distance could be perfectly derived from integrating the speed it there would be no need for additional along-localization methods. The idea is however that even if the integrated distance accumulates errors over time, the relative errors within a short segment of the signature will hopefully not have a significant impact on localization.

The spatially transformed signal is a non-uniformly sampled signal; the distance between two samples varies depending on the speed.

8.1.4 Spatial resampling

To facilitate processing it is desirable to have a uniformly sampled signal, so the next step is to resample the spatially transformed signal to obtain constant spatial sampling rate.

The resampling is performed by linear interpolation. Given the relatively high sampling rates, more advanced interpolation methods are deemed unlikely to give significant improvements.

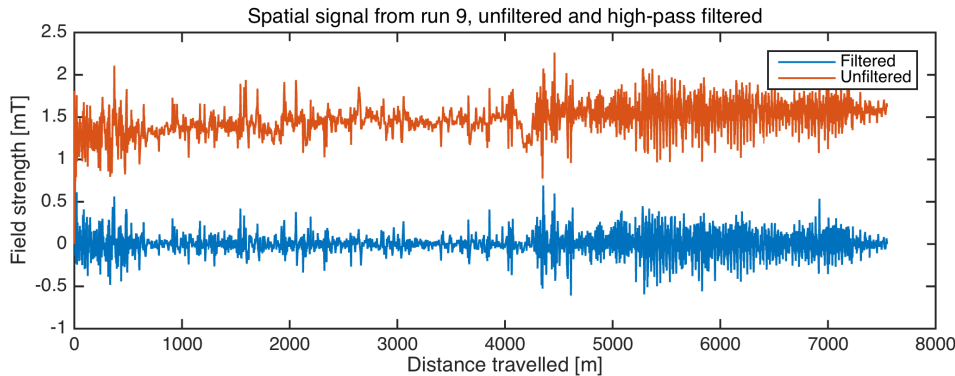


Figure 8.4: The spatially transformed and resampled magnetic magnitude signal is highpass-filtered in order remove slow-changing features and biases, but care is taken to preserve as much as possible of the short-wavelength information.

Another consideration in resampling is to avoid unnecessarily large amounts of data, as the resampling step discards a lot of the data collected in regions of slow speed. To speed up computations, a large spatial sampling distance is therefore desirable.

To choose a good spatial resampling rate several of the sharpest peaks in the signal were studied, and were found to be wider than one meter near the extremum. After some experimentation 0.25 m was chosen as a suitable spatial sampling rate.

8.1.5 Highpass-filtering

After resampling the signal is high-pass filtered. This is done to remove the influence of slow changes in the earth magnetic field and also sensor biases. The latter could of course also be dealt with in the temporal domain.

The filtering is performed by a butterworth-filter with cut-off wavelength of 25 m. Figure 8.4 illustrates the effect of the filtering, and Figure 8.5 shows the filter response as a function of wavelength.

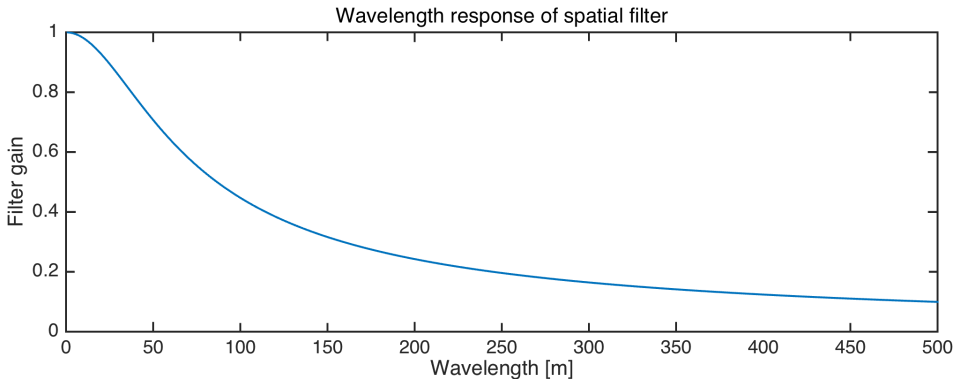


Figure 8.5: The spatial highpass-filtering means short wavelengths are passed through while longer wavelengths are attenuated.

8.2 Signature matching

The core of the proposed localization approach is to match the signature collected on-line, the localization signature, to a subsequence in the previously collected signature, the map signature.

Matching is performed by comparing the localization subsequence to all possible corresponding subsequences in the map, using some measure of similarity, as described by algorithm 1.

Algorithm 1 Signature matching

Input:

map_signature
localization_signature
similarity_measure (function)

Output:

index_of_match

```

1: siglength = length(localization_signature)
2: maplength = length(map_signature)
3:
4: for i = (siglength : maplength) do
5:   map_sequence = map_signature( (i-siglength+1) : i )
6:   score(i) = similarity_measure(localization_signature, map_sequence)
7: end for
8:
9: index_of_match = index_max(score)

```

8.2.1 Similarity measures

This section describes the different similarity measures used. All measures are chosen so that a value of zero means the signals are considered identical. In order to be able to compare signatures of different length, the values are normalized.

8.2.1.1 The L_1 - and L_2 measures

These two measures are obtained taking the difference between the signals, $\delta = x - y$, and applying an L_p -norm to it as defined by:

$$\|\delta\|_p = \left(\sum_{i=1}^n |\delta_i|^p \right)^{\frac{1}{p}}. \quad (8.3)$$

To obtain the similarity score the p -norm value is then normalized by the number of samples, n , with the corresponding p -root applied:

$$L_p(x, y) = \frac{\|\delta(x, y)\|_p}{n^{1/p}}. \quad (8.4)$$

The L_1 measure is thus simply the average difference per sample between the two signals, and the L_2 measure the square root of the average squared difference. The expression can be rewritten as:

$$L_p(x, y) = \left(\sum_{i=1}^n \frac{|x_i - y_i|^p}{n} \right)^{\frac{1}{p}}. \quad (8.5)$$

8.2.1.2 The correlation measure, C

This measure is basically one minus the (Pearson) correlation coefficient. The correlation coefficient, see Bronstein et al. [2013], is obtained by subtracting the means from the two signals and the taking their normalized scalar product:

$$C(x, y) = 1 - ((x - \bar{x}) \cdot (y - \bar{y}))_N. \quad (8.6)$$

The normalized scalar product is defined by

$$(x \cdot y)_N = \frac{\sum_{i=1}^n x_i \cdot y_i}{\sqrt{\sum_{i=1}^n x_i \cdot x_i} \sqrt{\sum_{i=1}^n y_i \cdot y_i}} \quad (8.7)$$

and has range minus one to one, $(x \cdot y)_N \in [-1, 1]$, which is why we define the correlation measure as one minus the correlation coefficient, obtaining a range from zero to two; $C(x, y) \in [0, 2]$.

8.3 Along-localization

Performing along-localization consists of applying the above methods of signature creation and matching, however there are some choices to be made in applying them. Algorithm 2 illustrates how they are applied and what parameters must be chosen.

Algorithm 2 Along-localization

Input:

position (current estimate)
localization_signature
map
search_radius

Output:

position (new estimate)

```
1: siglen = length(localization_signature)
2: map_signature = extract_sub_map(map, position, siglen, search_radius)
3:
4: match_index = match_signature(localization_signature, map_signature)
5:
6: position = lookup_position(map, match_index)
```

8.3.1 Localization signature length

The length of the localization signature, in meters, is of course a deciding factor for performance. If it is too short the signature will not contain enough information for good localization, if it is too long the results will start to suffer from signature distortions due to errors in the integrated speed.

8.3.2 Search radius

The search radius, in meters, determines how far away from the currently assumed position the algorithm will search for similar subsequences in the map signature.

If the currently assumed position is not very certain, then a larger search radius is needed. But increasing the search radius also increases the risk of false matches. The latter is a potential issue especially if there are repeating strong features in the track environment.

8.4 Across-localization

Across localization is the choice between two hypotheses, left and right, and is performed by using along-localization against signatures representing both hy-

potheses. The similarity score for each hypothesis can then be used as an indication of how likely it is.

To reduce the impact of disturbances each hypothesis is represented by multiple signatures, all along-localized against, and at each instant the best similarity score is used as the strength of the hypothesis.

Then the ratio of the two hypothesis strengths is used to indicate which one is more likely.

8.5 Reference position

In order to evaluate the localization performance the position estimates from the GNSS are used.

The quality of the GNSS position estimate varies with factors such as visibility of satellites and multi-path conditions where signals bounce off structures and thus appear to come from further away. After working with the data and comparing aerial photography, dashcam footage and signatures the authors estimate that the GNSS position is typically within 5 meters of the true position.

8.5.1 Map-matching

Since we know which path the train travelled over it is possible to eliminate some of the GNSS estimation error by projecting the GNSS position onto that path.

This is accomplished numerically by sampling the path at 0.1 m resolution and then using a nearest-neighbour search to associate each position with a position on the path. This introduces a quantization, and could possibly have other subtler effects. But as the railway paths are very smooth, such effects should have minimal effect.

9

Results

In this chapter we first describe our observations regarding the uniqueness and reproducibility of the signatures. Then we describe and try to quantify the performance of the localization methods.

9.1 Signature quality

Signatures are surprisingly similar between runs, the kind of similarity illustrated by Figure 9.1 is representative for the majority of the data. However, by visual inspection it quickly becomes clear that errors in integrated speed show up as distortions, illustrated in Figure 9.2.

9.1.1 Disturbances

If signature quality overall was very good, there were some instances of disturbances that severely degraded the signature in a small area. Trains passing nearby was the one cause of such disturbances, in Figure 9.4 signatures with and without a passing train is shown.

Semi-permanent changes in the magnetic environment that also seems to occur, although relatively infrequently, sometimes radically changing the signature, as shown in Figure 9.3. One likely cause for such changes are track maintenance, and especially track replacement.

9.1.2 Periodicity of features

Looking at the wavelength-spectrum of the spatial signal, shown in Figure 9.5, it is clear that there are some periodic features in the magnetic environment along the tracks.

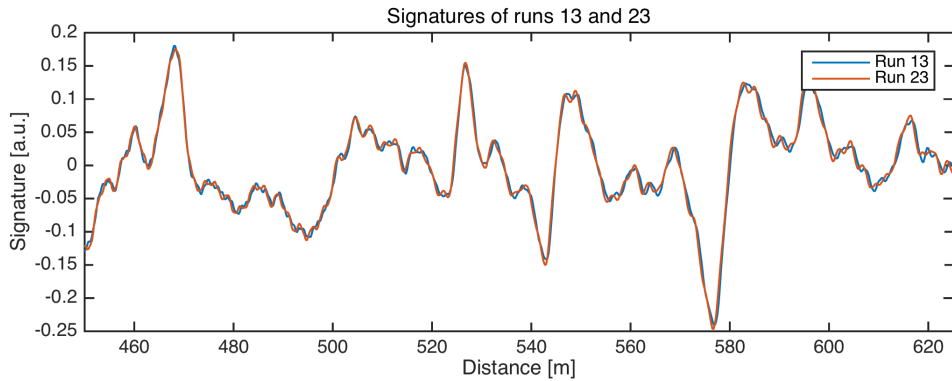


Figure 9.1: Mostly, signatures between different runs are very similar. Matching has been performed to align the signatures.

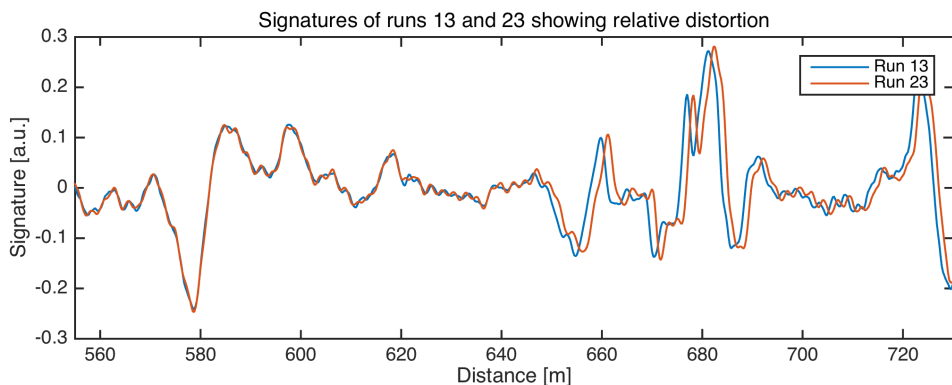


Figure 9.2: But sometimes errors in the integrated speed shows up as distortions.

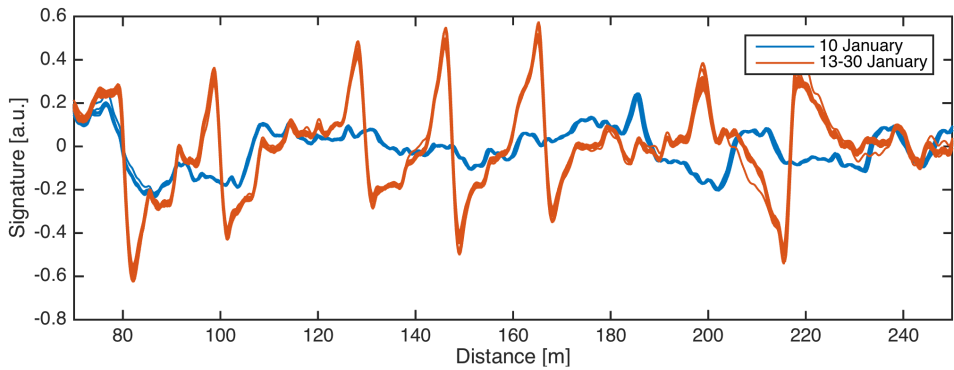


Figure 9.3: Features changing in the magnetic environment during the measurement campaign. Blue lines are 9 signatures from runs on the 10th of Januari. The red lines are 31 signatures collected between the 13th and 30th of January. One likely cause for the change would be track replacement.

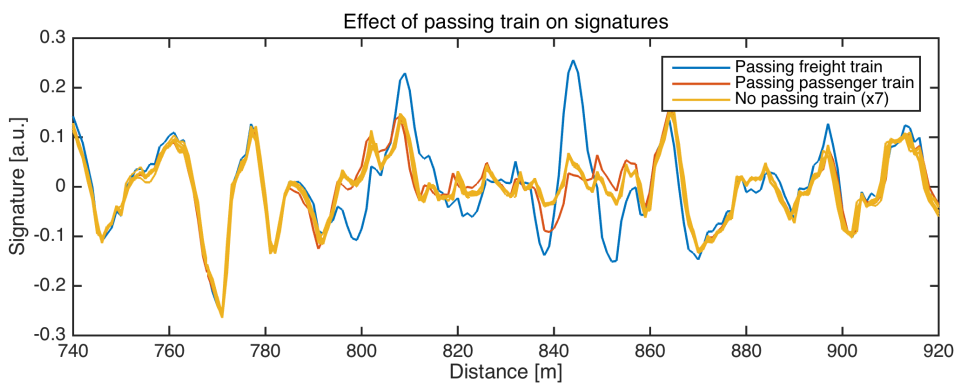


Figure 9.4: Passing trains on the same side as the magnetometer has relatively little impact on the signature.

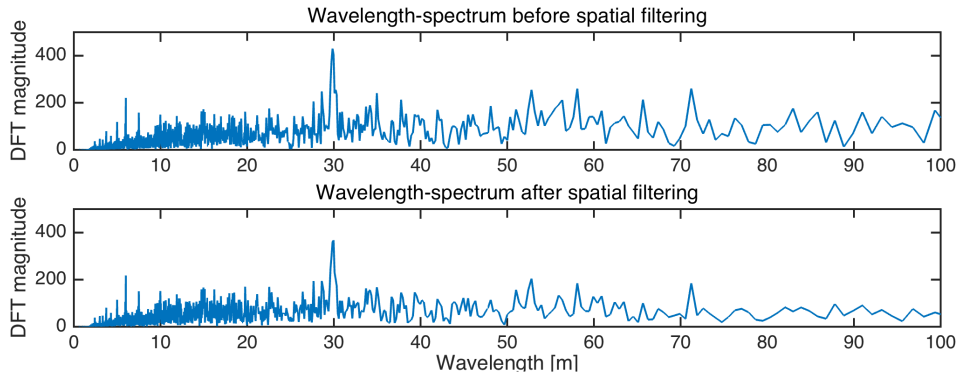


Figure 9.5: From the DFT of the spatially transformed signal it is clear that there are certain periodic features in the railway environment, the dominant type seems to have a wavelength of 30 m.

9.2 Along localization

9.2.1 Effect of localization signature length and search radius

Figure 9.6 illustrate the effect on localization performance obtained by of varying length and search radius. The similarity measure used is L_2 .

The benefits of using a longer localization signature start to level out at 30-40m where over 99% of localization estimates are within 5m of each other, using map-matched GNSS as a reference.

9.2.2 Comparison between similarity measures

Figures 9.7 and 9.7 show how the L_2 -measure performs compared to the L_1 and Correlation measure respectively. For short localization signatures (≤ 30 m) the L_2 -measure performs slightly better than both while it performs slightly worse than both for longer signatures. The differences are however very slight. The L_2 and L_1 measures are, perhaps unsurprisingly, the most similar, while the correlation measure differs somewhat by performing significantly worse for very short localization signatures.

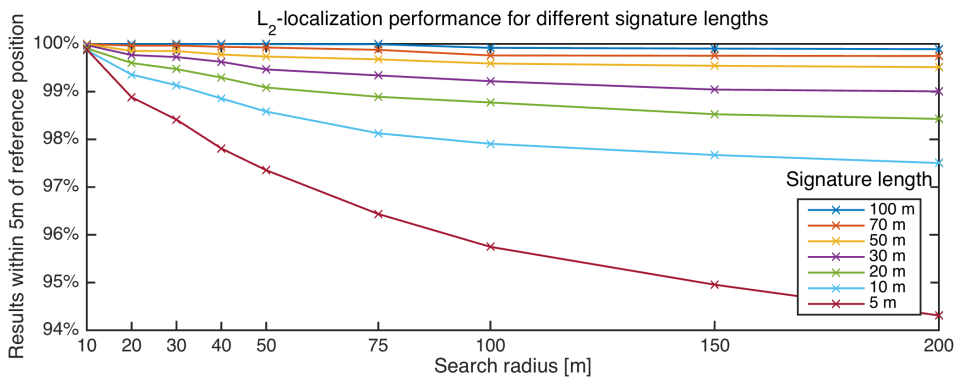


Figure 9.6: Results of L_2 -localization, showing percentage of results where the GNSS positions was within 5 m. Nine runs from the same day were used, to minimize impact of temporal changes, and every run was localized against every other run resulting in 72 pairs. The path was 6.8 km and localization was performed every meter.

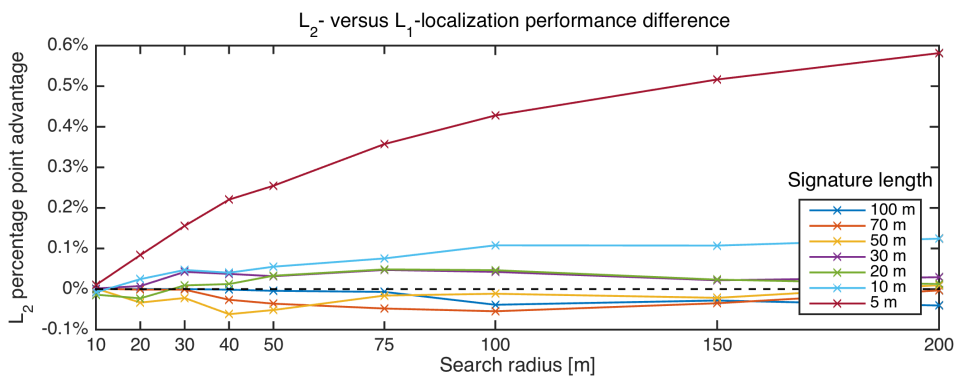


Figure 9.7: Performance difference between L_2 - and L_1 -localization. L_1 performs slightly better for signature lengths of 50 m or more.

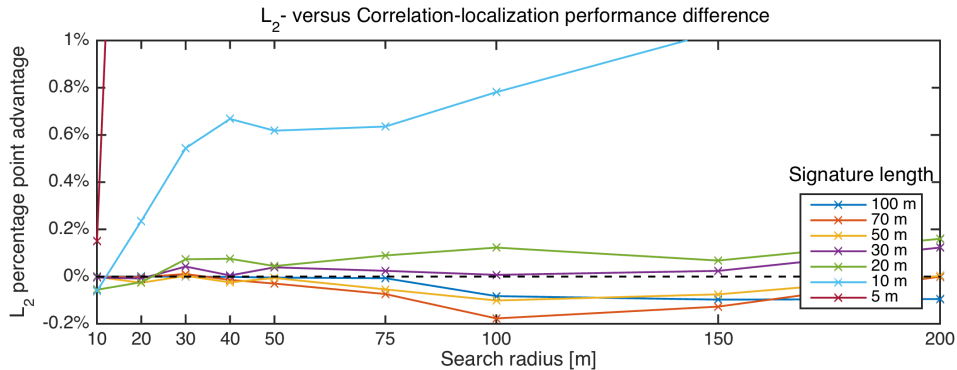


Figure 9.8: Performance difference between L_2 - and Correlation-localization. Correlation performs slightly better for signature lengths of 50 m or more. For 5 m signature length, Correlation performs significantly worse, about 13 percentage points at 50 m and 25 at 200 m search radius.

9.2.3 Impact of map-matching

As explained in Section 8.5.1, map-matching of the GNSS positions is used to improve accuracy. By comparing the position difference resulting from localization with and without map-matching one can get some notion of the impact of GNSS inaccuracy on the localization results. Figure 9.9 illustrates typical performance. The sharp peaks are caused by the GNSS-position suffering from so called multipath-drift when stationary.

It is clear that GNSS accuracy is a limiting factor in evaluating the performance of the method, as eliminating one part of that GNSS error dramatically improves results. The figure also illustrates how GNSS performance is very dependent on the environment.

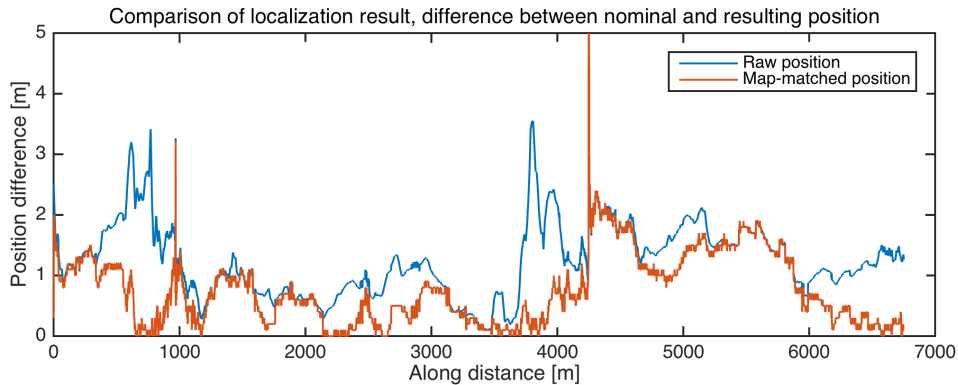


Figure 9.9: In areas of good GNSS-positioning the errors are consistently low, suggesting that much of the larger errors are caused by errors in the GNSS reference and that the underlying localization algorithm possibly has better accuracy.

9.3 Across localization

Across localization was performed with signature length 20 m and search radius 10 m, and performed well in the three switches studied. In all cases the strength ratio of the correct hypothesis to the incorrect was at least 5 after 40 m.

The results are shown in Figure 9.10, where a clear outlier can be seen in the Augsburg data. This comes from a semi-permanent change in the magnetic environment featuring in the signature used for localization being represented in one of the hypotheses but not in the other.

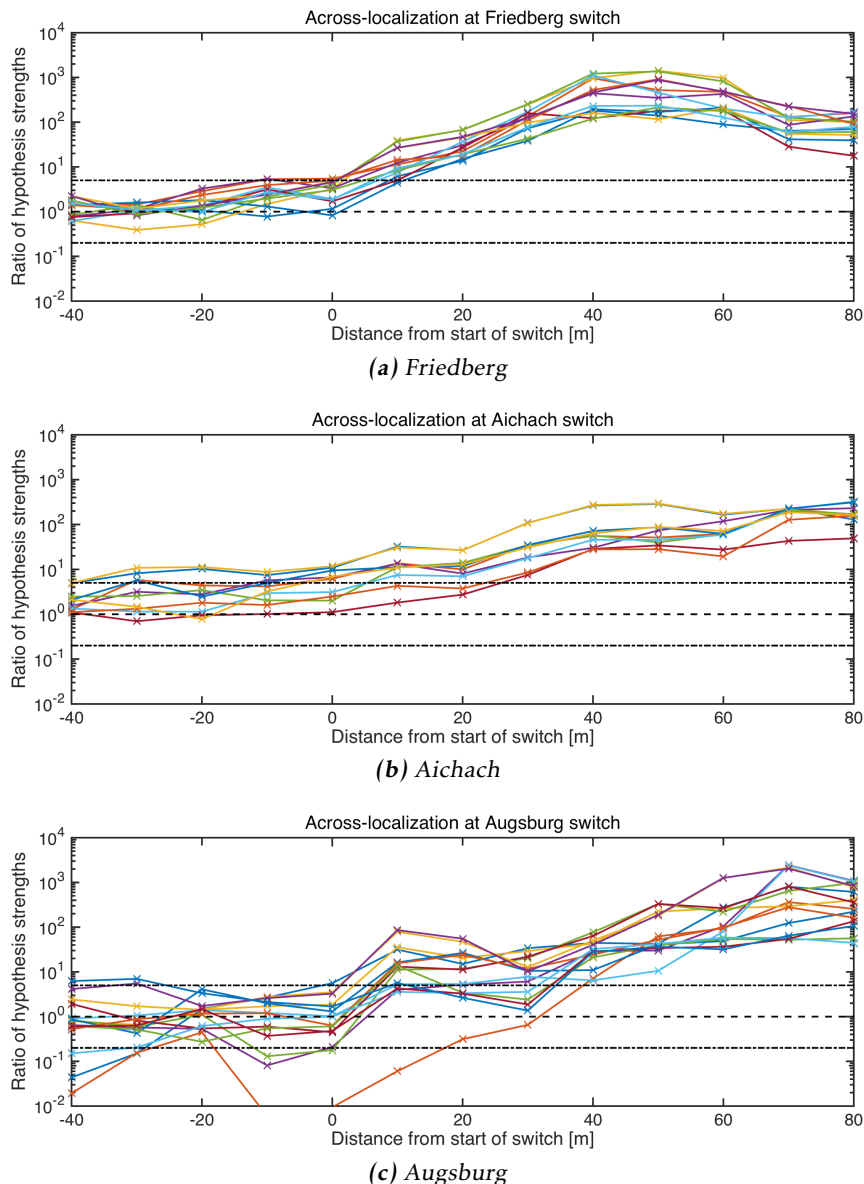


Figure 9.10: Results of across-localization at three different switches. The plotted values are the ratios between the similarity measures of the incorrect and the correct hypothesis, i.e. a value larger than 1 indicates that the correct hypothesis is considered most likely by the algorithm. In (c) the outlier is caused by changes in the magnetic signature.

10

Discussion

10.1 Along localization performance

It is clear that the magnetic environment along the railway tracks in question contain more than enough spatial uniqueness to provide the basis for very precise positioning. Various official targets for railroad navigation accuracy, see Durazo-Cardenas et al. [2014], are in the range of 2 to 3.5 m. The results suggest this kind of accuracy should be very possible to achieve using only measurements of the magnetic field combined with a good enough source of odometry.

As it stands, these methods would form a good complement to other estimators in a multisensor localization system since when disturbances occur they are of a "big bang" nature — easy to spot and therefore easy to handle e.g. by increasing estimate variance. In such a scenario the similarity scores could serve as a measure of estimation quality, a useful approach especially if historical similarity scores are used for comparison.

For increasing the stand-alone performance of these methods one promising area would be dynamic similarity measures.

10.2 Across localization performance

The results look promising, especially for such a basic method. Of course more data is needed in order to draw more general conclusions, but it is encouraging that the ratio of hypothesis strengths shows such similar behaviour in the three switches studied.

One thing that must be handled to achieve better performance is the problem

that arises when the magnetic environment changes, e.g. due to equipment replacement, and this change is only represented in one of the two hypotheses. It should be possible to identify such changes by comparing previous signatures and compensate for them.

10.3 Disturbances

At the start of the work passing trains were thought to be the largest difficulty, and while they do pose a problem, in our data track replacement or other infrastructure changes were the one causing the most loss of performance. This clearly shows that some kind of SLAM approach is need to identify changes and update the map signatures to use accordingly.

Part III

Concluding remarks

11

Concluding remarks

11.1 Summary

The first part of the thesis introduced speed estimation methods based on magnetic and inertial measurements respectively. The magnetic method performed well at speeds above 10 m/s, but was highly unreliable at lower speeds. The inertial method was not negatively affected by low speeds to the same extent, but performed noticeably worse overall. Both methods were incorporated into a Kalman-filter together with acceleration measurements in the direction of travel, yielding improved estimates.

The second part introduced methods for estimating location along a given track and for choosing between two possible tracks after passing a switch, both based on using magnetometer measurements and a speed estimate to create a magnetic signature. Both methods performed very well, as the signature proved to be surprisingly reproducible and unique. Infrequent but significant changes in the signature were identified as a problem.

Thus we conclude that there is enough speed- and location-dependent information in the sensor readings of the IMU to estimate the speed and position. The precision of the estimate depends on surrounding disturbances, but the estimates for both the speed and position look like promising candidates for inclusion into a multi-sensor system.

The thesis shows that good results can be achieved with relatively simple methods using low-cost low-maintenance on-board sensors.

11.2 Future work

The following are the areas the authors find most promising for further investigation.

11.2.1 Wheel maintenance

The wheel turn extraction method (see Section 4.1) estimates the speed by directly translating the wheel turn rate to an absolute speed for the train. This method relies on having a constant wheel diameter and that the wheels are not slipping. Since neither of the two are true (see Heirich et al. [2013b] and Lauer and Stein [2013]), there will be a bias in the speed estimations.

On the other hand, the signature matching method (see Section 4.2) is independent of wheel slip. By looking at the differences, this enables some wheel slip estimation and wheel diameter maintenance.

11.2.2 Estimated speed as input in the localization

The methods in the localization part relies on having a good speed input. As previously discussed, the GNSS-speed is not always so accurate. When the output from the speed estimation part is more stable, precise and quicker, this speed can be used as an input to the methods of localization to improve the results and also achieve a stand-alone solution.

11.2.3 Dynamic similarity measures

Using similarity measures that allow a certain distortion of the signals, so called dynamic similarity measures, would allow correction of, or maybe even completely replace, the currently used external speed estimate. This is also supported by some preliminary testing by the authors. Dynamic similarity measures are discussed in Section 7.2.2.

11.2.4 Pattern recognition

Pattern recognition applied either directly to the localization signature or to the difference between the map and the localization signatures would possibly enable identification passing trains and other typical disturbances. Identifying such features and removing their influence has the potential of making these methods very reliable, as the highly regulated track environment should mostly present disturbances of certain distinguishable types.

11.2.5 Incorporate inertial signals in the localization

In Weston et al. [2007] it is stated that bogie pitch rate is usable for localization, and preliminary tests by the thesis authors support this. The roll rate and vertical acceleration signals also show promise.

Appendix

A

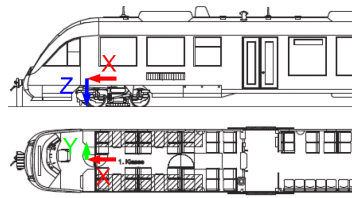
Sensor setup and technical data

This appendix shows the technical data over the sensors used to collect the data. The IMU sensor used was only the XSens MTi sensor (placed over the front wheel of the train).

Sensor positions

Reference

- X : Center of boogie, towards front
- Y : Center of track, towards right side of train
- Z : Height above rails, towards down
- Rotation: right hand, unit:rad, Z-Y-X DCM
- Resolution is cm (joint ruler meas.)

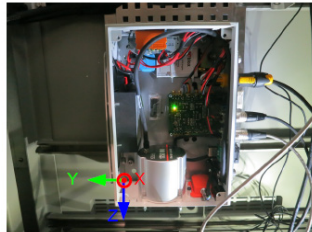


Boogie:

- Wheelbase: 1,89-1,90 m (Datasheet: 1,90m)
- Wheels: circumfence 2,38 m, R= 37,88 cm (Datasheet: 2,419m, d=770mm)

Box

- X (Backside): 1,10 m
- Y (Side with power unit): 1,03 m
- Z (Side with IMUs): 1,37 m



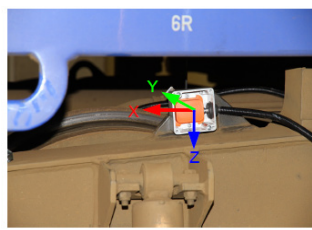
GPS antenna

- X (center of antenna): 1,52 m
- Y (center of antenna): 0 m
- Z (center of antenna): 3,63 m



IMU KVH (FOG)

- X (center of gravity ,cog): 1,17 m
- Y (cog) 0,92 m
- Z (cog): 1,40 m
- Roll: -3.131630137304843
- Pitch: -0.008866692062709
- Yaw: 0.785398163397448



IMU Xsens (MEMS, orange)

- X (acc center): 1,13 m
- Y (acc center): 0,88 m
- Z (acc center): 1,38 m
- Roll: 3.131758330491032
- Pitch: -0.010127055079816
- Yaw: 3.141592653589793

External Sensor

- X (center): 0,84 m
- Y (center, without lid) -0,95 m
- Z (center): 0,80 m
- Roll: -1.560411028777345
- Pitch: 0.000000059721063
- Yaw: -0.104988083498897

Figure A.1: Figure displaying the sensor positioning of the IMU sensors and the GNSS receiver with additional data.

Rotations:

- Rotation: right hand turn of axis (thumb direction axis, fingers indicate rotation)
- Right hand coordinate system: x (thumb) y (index finger) z (middle finger)
- ψ , psi is yaw is right hand rotation of z axis
- θ , theta is pitch is right hand rotation of y axis
- ϕ , phi is roll is right hand rotation of x axis
- Z-Y-X DCM (Direction Cosine Matrix)
- Following DCM is defined for the translation of the sensor data into the train frame:



$$\begin{aligned}
 R_{GS} &= R_y^Z R_y^Y R_y^X \\
 &= \begin{bmatrix} \cos\psi & -\sin\psi & 0 \\ \sin\psi & \cos\psi & 0 \\ 0 & 0 & 1 \end{bmatrix} \begin{bmatrix} \cos\theta & 0 & \sin\theta \\ 0 & 1 & 0 \\ -\sin\theta & 0 & \cos\theta \end{bmatrix} \begin{bmatrix} 1 & 0 & 0 \\ 0 & \cos\phi & -\sin\phi \\ 0 & \sin\phi & \cos\phi \end{bmatrix} \\
 &= \begin{bmatrix} \cos\theta\cos\psi & \sin\phi\sin\theta\cos\psi - \cos\phi\sin\theta\cos\psi & \cos\phi\sin\theta\cos\psi + \sin\phi\sin\psi \\ \cos\theta\sin\psi & \sin\phi\sin\theta\sin\psi + \cos\phi\cos\psi & \cos\phi\sin\theta\sin\psi - \sin\phi\cos\psi \\ -\sin\theta & \sin\phi\cos\theta & \cos\phi\cos\theta \end{bmatrix}
 \end{aligned}$$

As defined here R_{GS} rotates a vector in the sensor co-ordinate system (S) to the global reference system (G):

$$\mathbf{x}_G = R_{GS} \mathbf{x}_S = (R_{GS})^T \mathbf{x}_S$$

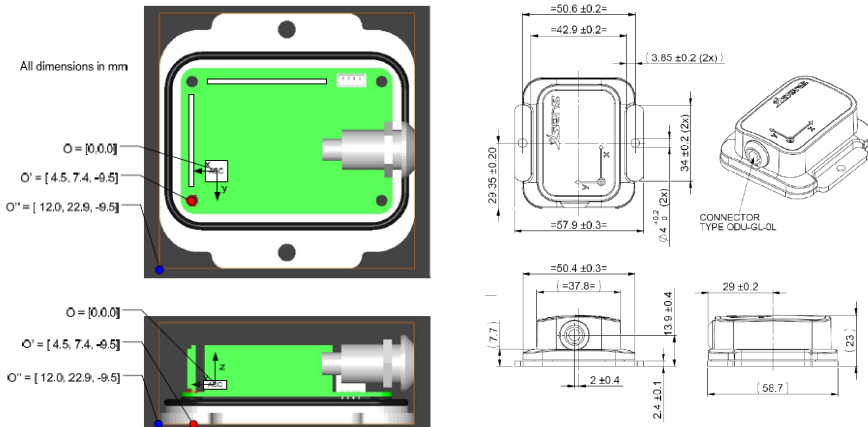
IMU Xsens MTi

Figure A.2: Technical data for the Xsens-MTi sensor. This sensor was the one above the wheel.

Bibliography

- V. Augutis, D. Gailius, R. Misevičius, and V. Pronko. Analysis of Influence of Disturbing Signals Caused by Rail Magnetization to a Cab Signaling System. *Elektronika ir Elektrotechnika*, 101(5):103–106, 2015.
- I.N. Bronstein, K.A. Semendjajew, G. Musiol, and H. Mühlig. *Taschenbuch der Mathematik*. Verlag Europa-Lehrmittel, 9 edition, 2013. ISBN 978-3-8085-5671-9.
- A. Chulliat, S. Macmillan, P. Alken, C. Beggan, M. Nair, B. Hamilton, A. Woods, V. Ridley, S. Maus, and A. Thomson. The US/UK World Magnetic Model for 2015-2020. 2015. doi: 10.7289/V5TB14V7.
- H. Ding, G. Trajcevski, P. Scheuermann, X. Wang, and E. Keogh. Querying and mining of time series data: experimental comparison of representations and distance measures. *Proceedings of the VLDB Endowment*, 1(2):1542–1552, 2008.
- I. Durazo-Cardenas, A. Starr, A. Tsourdos, M. Bevilacqua, and J. Morineau. Precise Vehicle Location as a Fundamental Parameter for Intelligent Self-aware Rail-track Maintenance Systems. *Procedia CIRP*, 22:219–224, 2014. ISSN 22128271. doi: 10.1016/j.procir.2014.07.002.
- S. Grassie. Measurement of railhead longitudinal profiles: a comparison of different techniques. *Wear*, 1996(191):245–251, 1996.
- F. Gustafsson. *Statistical Sensor Fusion*. Studentlitteratur, first edition, 2012.
- F. Gustafsson, L. Ljung, and M. Millnert. *Signal Processing*. Studentlitteratur, first edition, 2011.
- O. Heirich and B. Siebler. Train-side passive magnetic measurements. In *IEEE International Instrumentation and Measurement Technology Conference (I2MTC)*, Pisa, Italy, may 2015.
- O. Heirich, A. Lehner, P. Robertson, and T. Strang. Measurement and analysis of train motion and railway track characteristics with inertial sensors. In *14th*

- International IEEE Conference on Intelligent Transportation Systems (ITSC)*, oct. 2011.
- O. Heirich, P. Robertson, and T. Strang. RailSLAM - Localization of Rail Vehicles and Mapping of Geometric Railway Tracks. In *International Conference on Robotics and Automation, IEEE ICRA*, Mai 2013a.
- O. Heirich, A. Steingass, A. Lehner, and T. Strang. Velocity and location information from onboard vibration measurements of rail vehicles. In *Information Fusion (FUSION), 2013 16th International Conference on*, July 2013b.
- S. Hensel, C. Hasberg, and C. Stiller. Probabilistic Rail Vehicle Localization With Eddy Current Sensors in Topological Maps. *IEEE Transactions on Intelligent Transportation Systems*, 12(4):1525–1536, December 2011. ISSN 1524-9050. doi: 10.1109/TITS.2011.2161291.
- M. Lauer and D. Stein. Algorithms and concepts for an onboard train localization system for safety-relevant services. In *Intelligent Rail Transportation (ICIRT), 2013 IEEE International Conference on*, pages 65–70. IEEE, 2013.
- L. Ljung and T. Glad. *Modellbygge och simulering*. Studentlitteratur, second edition, 2011.
- M. Malvezzi, B. Allotta, and M. Rinchi. Odometric estimation for automatic train protection and control systems. *Vehicle System Dynamics*, 49(5):723–739, May 2011. ISSN 0042-3114, 1744-5159. doi: 10.1080/0042311003721291.
- T. X. Mei and H. Li. Monitoring train speed using bogie mounted sensors—Accuracy and robustness. In *Railway Condition Monitoring, 2008 4th IET International Conference on*, pages 1–6. IET, 2008.
- M. Müller. *Information retrieval for music and motion*. Springer, New York, 2007. ISBN 9783540740476.
- NOAA. NCEI Magnetic Field Calculators, 2015. URL <http://www.ngdc.noaa.gov/geomag-web/>.
- K.P. Subbu, B. Gozick, and R. Dantu. Indoor localization through dynamic time warping. In *Systems, Man, and Cybernetics (SMC), 2011 IEEE International Conference on*, pages 1639–1644. IEEE, 2011.
- C. Swett. Outpatient phenothiazine use and bone marrow depression. A report from the drug epidemiology unit and the Boston collaborative drug surveillance program. *Archives of General Psychiatry*, 32(11):1416–1418, November 1975. ISSN 0003-990X.
- H. Tsunashima, A. Matsumoto, H. Mori, T. Mizuma, and Y. Naganuma. *Condition monitoring of railway track using in-service vehicle*. INTECH Open Access Publisher, 2012.
- P. Weston, C. Ling, C. Roberts, C. Goodman, P. Li, and R. Goodall. Monitoring vertical track irregularity from in-service railway vehicles. *Proceedings of the*

Institution of Mechanical Engineers, Part F: Journal of Rail and Rapid Transit, 221(1):75–88, January 2007. ISSN 0954-4097. doi: 10.1243/0954409JRRT65.



Upphovsrätt

Detta dokument hålls tillgängligt på Internet — eller dess framtida ersättare — under 25 år från publiceringsdatum under förutsättning att inga extraordinära omständigheter uppstår.

Tillgång till dokumentet innebär tillstånd för var och en att läsa, ladda ner, skriva ut enstaka kopior för enskilt bruk och att använda det oförändrat för icke-kommersiell forskning och för undervisning. Överföring av upphovsrätten vid en senare tidpunkt kan inte upphäva detta tillstånd. All annan användning av dokumentet kräver upphovsmannens medgivande. För att garantera äktheten, säkerheten och tillgängligheten finns det lösningar av teknisk och administrativ art.

Upphovsmannens ideella rätt innehåller rätt att bli nämnd som upphovsman i den omfattning som god sed kräver vid användning av dokumentet på ovan beskrivna sätt samt skydd mot att dokumentet ändras eller presenteras i sådan form eller i sådant sammanhang som är kränkande för upphovsmannens litterära eller konstnärliga anseende eller egenart.

För ytterligare information om Linköping University Electronic Press se förlagets hemsida <http://www.ep.liu.se/>

Copyright

The publishers will keep this document online on the Internet — or its possible replacement — for a period of 25 years from the date of publication barring exceptional circumstances.

The online availability of the document implies a permanent permission for anyone to read, to download, to print out single copies for his/her own use and to use it unchanged for any non-commercial research and educational purpose. Subsequent transfers of copyright cannot revoke this permission. All other uses of the document are conditional on the consent of the copyright owner. The publisher has taken technical and administrative measures to assure authenticity, security and accessibility.

According to intellectual property law the author has the right to be mentioned when his/her work is accessed as described above and to be protected against infringement.

For additional information about the Linköping University Electronic Press and its procedures for publication and for assurance of document integrity, please refer to its www home page: <http://www.ep.liu.se/>